Received: 25 November 2022 | Revised: 13 March 2023 | Accepted: 12 April 2023

DOI: 10.1002/mp.16436

RESEARCH ARTICLE

MEDICAL PHYSICS

Automated isocenter optimization approach for treatment planning for gyroscopic radiosurgery

Carolin Stapper[1] | **Stefan Gerlach**[1] | **Theresa Hofmann**[2] | **Christoph Fürweger**[2] | **Alexander Schlaefer**[1]

[1]Institute of Medical Technology and Intelligent Systems, Hamburg University of Technology, Hamburg, Germany

[2]European Radiosurgery Center Munich, Munich, Germany

Correspondence
Carolin Stapper.
Email: carolin.stapper@tuhh.de

Funding information
Deutsche Forschungsgemeinschaft, Grant/Award Numbers: SCHL1844/3-2, SCHL1844/6-1

[Correction added on 2 June, 2023 after first online publication: the fourth author name is updated to Fürweger.]

Abstract

Background: Radiosurgery is a well-established treatment for various intracranial tumors. In contrast to other established radiosurgery platforms, the new ZAP-X® allows for self-shielding gyroscopic radiosurgery. Here, treatment beams with variable beam-on times are targeted towards a small number of isocenters. The existing planning framework relies on a heuristic based on random selection or manual selection of isocenters, which often leads to a higher plan quality in clinical practice.

Purpose: The purpose of this work is to study an improved approach for radiosurgery treatment planning, which automatically selects the isocenter locations for the treatment of brain tumors and diseases in the head and neck area using the new system ZAP-X®.

Methods: We propose a new method to automatically obtain the locations of the isocenters, which are essential in gyroscopic radiosurgery treatment planning. First, an optimal treatment plan is created based on a randomly selected nonisocentric candidate beam set. The intersections of the resulting subset of weighted beams are then clustered to find isocenters. This approach is compared to sphere-packing, random selection, and selection by an expert planner for generating isocenters. We retrospectively evaluate plan quality on 10 acoustic neuroma cases.

Results: Isocenters acquired by the method of clustering result in clinically viable plans for all 10 test cases. When using the same number of isocenters, the clustering approach improves coverage on average by 31 percentage points compared to random selection, 15 percentage points compared to sphere packing and 2 percentage points compared to the coverage achieved with the expert selected isocenters. The automatic determination of location and number of isocenters leads, on average, to a coverage of $97 \pm 3\%$ with a conformity index of 1.22 ± 0.22, while using 2.46 ± 3.60 fewer isocenters than manually selected. In terms of algorithm performance, all plans were calculated in less than 2 min with an average runtime of 75 ± 25 s.

Conclusions: This study demonstrates the feasibility of an automatic isocenter selection by clustering in the treatment planning process with the ZAP-X® system. Even in complex cases where the existing approaches fail to produce feasible plans, the clustering method generates plans that are comparable to those produced by expert selected isocenters. Therefore, our approach

can help reduce the effort and time required for treatment planning in gyroscopic radiosurgery.

KEYWORDS
gyroscopic radiosurgery, radiation therapy, treatment planning, ZAP-X

1 | INTRODUCTION

Due to the focused delivery of radiation dose with beams from many directions, radiosurgery has been shown to be an effective treatment method for intracranial tumors.[1,2] While systems such as the Gamma Knife and CyberKnife are commonly used to treat these tumors, the cost of treatment devices and their installation, including the installation of a vault, is often prohibitive. Recently, vault-free, gyroscopic radiosurgery has been proposed, which can reduce cost due to lower treatment facility requirements.[3] However, current treatment planning approaches for gyroscopic treatment are still limited regarding treatment plan quality and ease of use for more irregularly shaped targets.

In general, treatment planning is highly dependent on the treatment device and its capability to shape dose distributions. With the CyberKnife, the LINAC is moved by a serial robot, which allows for high flexibility in dose delivery.[4,5] A cylindrical collimator or a multileaf collimator is mounted in front of the beam source to shape the beam. The serial robot allows for beams to be nonisocentric and noncoplanar, which can improve the treatment plan quality.[6,7] Approaches for inverse optimization usually include solving a linear[8] or nonlinear optimization problem[9] to select and weight optimal beams.

With the Gamma Knife, radiation beams are produced in parallel by 192 sources of cobalt-60, converging at the isocenter.[10] During treatment, the isocenter is moved to treat the complete target. However, achievable dose distributions are limited by the isotropic nature of the beam delivery. Each shot delivers a dose distribution, which approximates a sphere. Therefore, first treatment planning approaches used sphere packing to find the optimal number and location of isocenters,[11–13] which has recently been extended with an inverse optimization algorithm.[14,15]

The ZAP-X (ZAP Surgical System, San Carlos, USA) is a newly developed therapeutic radiotherapy device that is dedicated to the stereotactic radiosurgery of the brain and the head and neck. It is based on a gyroscopically moved LINAC, which can be rotated in 2 DOF on a sphere around the patient's head to enable delivery from different beam directions.[3] Beam collimation is achieved by a collimator wheel with spherical apertures producing beam diameters of 4–25 mm.

In contrast to the Gamma Knife, beams targeting the same isocenter can have different beam-on time. Therefore, the system promises to allow for more complex dose distributions compared to the Gamma Knife. Besides, the ZAP-X is able to translate the isocenter by moving the patient couch in 3 DOF. In contrast to CyberKnife treatments, the ZAP-X currently relies on a limited number of isocenters in practice in order to minimize the number of couch movements and the associated delay due to image guidance. Current treatment planning relies on a randomized heuristic to find the number and location of isocenters. However, manual selection of isocenter locations often leads to higher plan quality in clinical practice.[16]

In this study, we introduce a novel approach for automatic isocenter selection based on clustering to improve plan quality and reduce the planning effort.

For comparison, we implement a sphere packing approach based on target geometry previously presented for the ZAP-X,[17] as well as a random approach that resembles the heuristics currently implemented in the ZAP-X treatment planning system. We assess plan quality and clinical feasibility of the proposed method compared to these existing isocenter placing methods and manual placement by medical experts on 10 different acoustic neuroma patient cases, which have previously been treated with the ZAP-X system.

2 | METHODS

2.1 | Treatment planning

For inverse treatment planning, we adapt our previously proposed planning framework based on linear programming.[8] Three dimensional contoured volumes of interest (VOIs), namely the planning target volume (PTV) and organs at risk (OARs), are delineated by medical experts using CT scans and secondary image data such as contrast-enhanced T1-weighted MRIs. Additional shell structures around the PTV are defined to control the dose gradient in normal tissue. The goal of treatment planning is then to find a configuration of beams that deliver the prescribed dose to the PTV while constraining the dose to OARs and shells.

The setup of the optimization can be separated into sequential steps. First, a large number of candidate beams are randomly sampled. Here, we ensure deliverability of the beam set with regard to collisions as further detailed in the following sections. The dose per beam

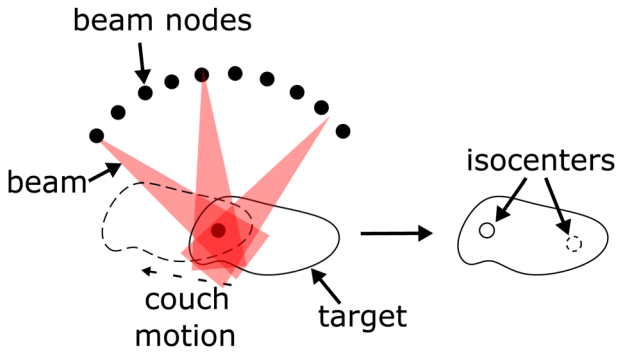

FIGURE 1 Schematic illustration of possible directions for dose delivery. The isocenter location is changed by a motion of the patient couch. Dashed target position corresponds to the dashed isocenter.

in a given voxel of the CT scan is calculated using an equivalent path length algorithm.[18]

These coefficients represent the dose per beam weight delivered by a beam at a given location in the CT. We optimize for PTV coverage by minimizing underdosage of voxels in the PTV. We specify hard constraints on the maximum dose in PTV, OARs and the shells, as well as the maximum number of monitor units (MU). The optimization results in a weighted subset of the candidate beams. Here, each beam's weight corresponds to the activation time of the respective beam.

2.2 | Isocenter optimization

With the ZAP-X, dose can be delivered from beam nodes which are distributed on a sphere around an isocenter as shown in Figure 1. To reposition the target and thus change the position of the isocenter, the patient couch must be moved. Since this leads to positional uncertainty, stereoscopic kV-images are acquired by the ZAP-X system after each couch shift, which takes approximately 30 s. For each isocenter, a change of the beam source location involves rotary motion of the LINAC, which is realized considerably faster. Therefore, the number of isocenters that are used during treatment should be small. Currently, the ZAP-X does not change the collimator size during delivery of beams for a particular isocenter. While the system can quickly change the collimator, current treatment plans do not fully utilize this capability. For fair comparison, we also allow only one collimator size per isocenter.

In order to generate the isocenter locations automatically, we look at three different methods to generate a specified number of isocenters N: clustering, sphere packing, and random generation. To compare the expert-selected isocenters with the automatically constructed ones, we also load these isocenters into our framework and create beams for each isocenter as described in Section 2.3.

2.2.1 | Clustering

We propose a heuristic based on clustering to determine the location of isocenters as shown in Figure 2. First, a large set of nonisocentric beams is randomly generated. The generation process is analogous to the one described in Section 2.3. The beam source locations are placed on a sphere centered on the PTV centroid instead of an isocenter. Beam targets are not limited to isocenters, but are randomly sampled within the PTV. The collimator size is arbitrarily selected from the available options. Because the number of possible combinations is greatly increased by these modifications, we limit the number of considered beams to $n_b = 6000$, which are selected randomly.

This beam set is then optimized, resulting in a weighted beam set B. Here, the weighted beams ($w_b > 0$) correspond to the beams that were selected due to optimization. Note that these beams cannot be directly delivered practically by the ZAP-X as the realization of many different isocenters leads to unfeasible treatment times. However, they represent promising directions for dose delivery and are the basis for the selection of isocenters. Next, the weighted beam set is split into separate beam sets for each collimator size B_{col} to determine optimal isocenters for each collimator size.

First, we determine an optimal potential isocenter i_p for each pair of beams. It corresponds to the intersection point or the midpoint of the shortest connections between the beams for intersecting or skew beams, respectively.

Parallel or identical pairs of beams are not considered. Each i_p is assigned a corresponding weight $w = w_1 * w_2 * (1 - d/d_{max})$ depending on the weights w_1 and w_2 of the beam pair and their shortest distance d to i_p. If d is greater than $d_{max} = 5$ mm the weight is set to zero.

All points i_p are then clustered using the weighted k-means method.[19] Here we use the weighted Euclidean distance in the objective function. Synthetic starting point values are assigned based on the scrambled midpoints method.[20] The number of clusters per collimator size N_{col} is determined to reflect its relative contribution to the initial solution.

$$N_{col} = round\left(N * \frac{|B_{col}|}{|B|}\right) \quad (1)$$

2.2.2 | Sphere packing

For comparison with our clustering method, we implement a sphere packing approach similar to the one introduced by Adler,[17] which was initially implemented in the ZAP-X planning framework. It is a heuristic sphere-packing approach where spheres are packed

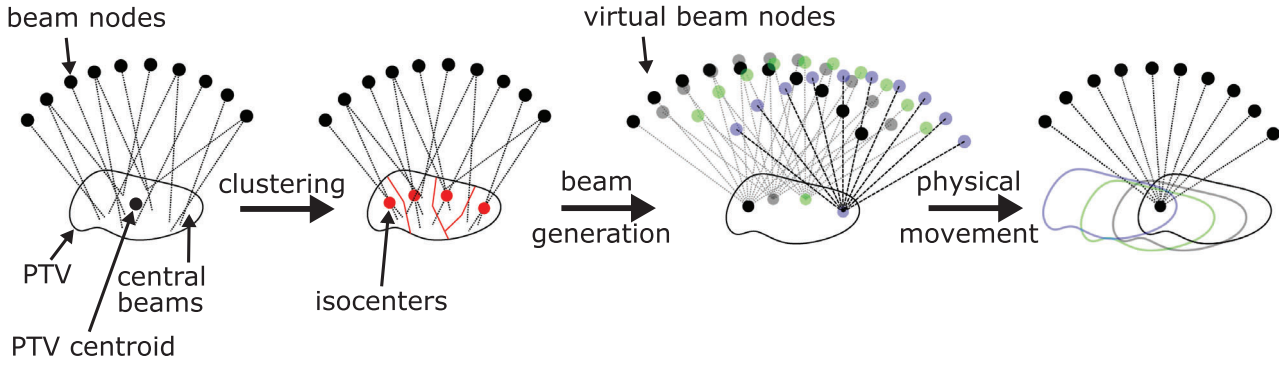

FIGURE 2 2D repr esentation of the clustering approach. Note that only weighted beams are considered for clustering. In 3D, central beams usually do not intersect. We consider the points of closest distance to determine isocenters.

one-by-one with largest possible collimator size, located such that they cover as many surface voxels as possible of the not already covered PTV.

The first step is to perform a distance transform using the grassfire algorithm.[21] Afterwards, the resulting voxel labels are reversed such that surface voxels have the highest and center voxels have the lowest values.

Starting with the largest collimator size as the sphere diameter, we first extract all voxel centers within the current target volume that can be considered as sphere centers. Thereby, the sphere must not cover healthy tissue or intersect an already placed sphere. Each extracted sphere center is now assigned a score equal to the sum of the voxel labels covered by the sphere. The center with the highest score is chosen as the isocenter.

Following the creation of the new sphere, all voxels contained within it are removed from the current target volume. The algorithm is then repeated. If no more spheres of the current collimator size fit into the remaining volume, the next smaller one is chosen. The algorithm terminates as soon as the N spheres are packed or all voxels of target volume are covered by a sphere.

2.2.3 | Random generation

The random generation method emulates the heuristics currently implemented in the treatment planning system. It employs the simple approach of randomly selecting voxels within the PTV whose centers are chosen as isocenters. However, only certain voxels are considered depending on the collimator size. For this, a collimator diameter d is first randomly selected from the available collimators. Then, the PTV is eroded by $0.6d$. Finally, a voxel from the surface of the eroded volume is randomly selected as the isocenter voxel.

2.3 | Beam generation

After generating the isocenters and associated collimators, the candidate beam set is generated. For this purpose, possible source positions are generated for each isocenter-collimator pair as shown on the right part of Figure 2. These sources are located on a sphere at 450-mm distance from the isocenter and are subsampled in discrete angle steps. Source positions that lead to a collision of the LINAC with the patient or the system set-up are discarded. We evaluate for collision by using convex models for the patient couch, patient, and LINAC.

During the beam generation process, all combinations of isocenter-collimator pairs and their associated sources are set as the beams target point, collimator, and source location, respectively.

2.4 | Number of isocenters

The presented methods generate a prespecified number N of isocenters. To determine this number automatically within the clustering method the pseudo-F statistic[22] is considered. For each collimator size, we cluster the beams with increasing number of clusters N_{col}. We use the cluster size N_{col} maximizing the pseudo-F index

$$pF = \frac{BSS}{WSS} \cdot \frac{W - N_{col}}{N_{col} - 1}, \tag{2}$$

with BSS being the between cluster weighted squared distance, WSS the within cluster weighted squared distance and $W = \sum_{b \in B_{col}} w_b$. In order to reduce the resulting isocenter number N, an additional pruning step is introduced after the optimization. An isocenter is removed if the total weight of its assigned beams is below the threshold $\frac{\sum w_b}{k \cdot N}$. Based on preliminary evaluation, we found that $k = 1.5$ leads to the best results. With the reduced isocenter set, a final optimization step is performed that results in the treatment plan.

TABLE 1 Case overview stating the volume of the PTVs, selected number of isocenters N_{ref} and used monitor units (MU).

Case	Volume [cc]	N_{ref}	Total MU
1	0.115	3	8341
2	0.377	13	12 005
3	0.507	6	7946
4	0.532	11	11 762
5	0.626	6	7841
6	0.944	11	7791
7	1.289	7	8341
8	2.356	13	12 583
9	3.608	18	12 332
10	5.125	11	12 583

2.5 | Patient data

Our data set consists of 10 patient cases that were previously treated for acoustic neuroma with the ZAP-X System (Table 1). Due to their mostly nonspherical shape, acoustic neuromas present an interesting optimization problem with respect to isocenter placement. For the treatment, the isocenters were selected manually by the operator of the system. Their number is referred to as N_{ref} in the following. All cases have a prescribed dose of 13 Gy. The target shape and size covers a wide range with volumes from 0.115 to 5.125 cc. N_{ref} ranges from 2 to 18 with more complex and larger targets generally requiring more isocenters for sufficient coverage. We define the cochlea and the brainstem as OARs, both with a maximum dose of 8 Gy. The PTVs maximum dose is set to 22 Gy.

2.6 | Experimental setup

To evaluate the presented methods, the plans are optimized with different parameters.

To achieve a steep dose decay, two shells are placed around the PTV at a distance of 3 and 9 mm. The dose limits of those shells are parameterized such that the reference beam set derived with the manually selected isocenters results in a coverage of 95%. Each beam can have a maximum MU of 300. The limit of total MU is set to 12 000.

The primary optimization goal is to maximize the coverage of the PTV. In a second optimization step, the mean dosage inside the two shells is minimized while keeping the achieved coverage to improve the conformity of the plans. We use 30 different seeds to produce 30 plans for each patient and isocenter generation method.

We evaluate the plans based on coverage, and dosimetric quality measures such as the new conformity index ($nCI = \frac{PTV \cdot PIV}{PTV_{PIV}^2}$), homogeneity index ($HI = \frac{D_{max}}{D_{min}}$) and gradient index ($GI = \frac{PIV_{0.5}}{PIV}$).[23–25] PIV is the total tissue volume that receives at least the prescribed dose, PTV_{PIV} is the tumor volume that receives at least the prescribed dose. $PIV_{0.5}$ is the total tissue volume receiving at least half the prescribed dose. D_{max} and D_{min} are the maximum and minimum dose in the tumor.

TABLE 2 Index statistics for $N = N_{ref}$.

	Reference	Cluster	Random	Sphere
CO	0.95	0.97 ± 003	0.66 ± 025	0.82 ± 012
nCI	1.24 ± 018	1.29 ± 027	1.67 ± 070	1.40 ± 029
HI	2.13 ± 037	2.11 ± 036	3.21 ± 101	2.84 ± 078
GI	2.05 ± 022	1.92 ± 018	2.61 ± 084	2.21 ± 025

Abbreviations: CO, coverage; GI, 50% gradient index; HI, homogeneity index; nCI, new conformity index.

3 | RESULTS

First, we present the results for the proposed isocenter generation method depending on the number of isocenters compared to the existing approaches and the manually selected isocenters for the 10 patient cases. Then, we focus on two patients for a more in-depth analysis of our results. Finally, we examine the treatment plan results when the number of isocenters is determined automatically by the clustering algorithm and compare the runtimes of the three isocenter generation methods.

3.1 | Fixed number of isocenters

The resulting coverage of all created plans for the 10 cases is displayed in Figure 3. The coverage increases with increasing number of isocenters. Overall, clustering achieves the best coverage. With sphere packing, the first placed spheres result in good initial coverage compared to the other methods, but the method reaches a plateau around 85% coverage starting at 10 isocenters, where coverage does not increase with more isocenters. The random generation outperforms the sphere packing with respect to coverage for 17 or more isocenters.

To compare the three isocenter generation methods with the results from the manually selected reference isocenter set, N is set to N_{ref} for each case. Table 2 shows the resulting coverage and index statistic averaged over all created plans.

With the clustering method, the average coverage of 97% is higher compared to the reference with a low standard deviation of 3 pp. For two of the 10 patients, the coverage is 94% and therefore below the reference. Sphere packing reaches 82% coverage on average. A coverage above 95% is achieved for the three

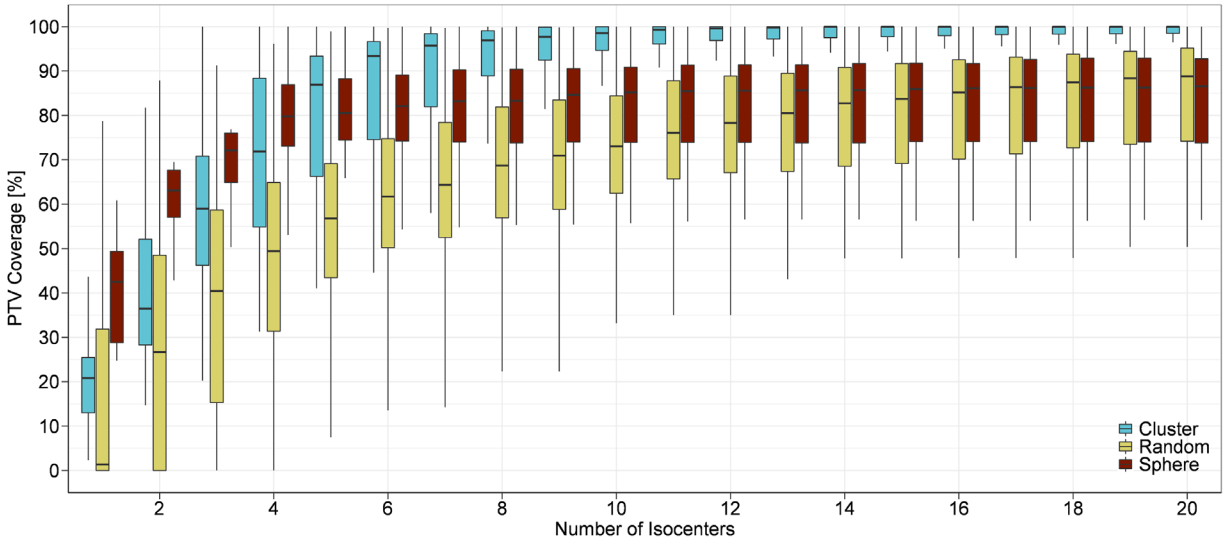

FIGURE 3 PTV coverage across all 10 patients depending on generation method and number of isocenters. Deviation is due to different results for each patient. Additional variation is due to the use of different random seeds for clustering and random isocenter generation. PTV, planning target volume.

TABLE 3 Required number of isocenters to reach reference coverage.

	Cluster	Random	Sphere
ΔN	-1.70 ± 284	$+9.38 \pm 707$	-1.81 ± 125
# not reached	0	3	7

$\Delta N = N_{ref} - N_{0.95}$ is calculated for all cases where the reference coverage of 95% is achieved with a maximum of 50 isocenters.

smallest PTVs. In all other cases, coverage varies between 55 and 91%. The random generation does not reach the reference coverage in any of the 10 cases. It varies between 17 and 85% with an average of 66%.

The conformity index of clustering is slightly worse than the reference, while homogeneity and gradient index are both lower than the reference index. Both sphere packing and random generation result in larger values for all three indices. The random generation's high conformity and gradient index results from cases with very small PIV and TTV.

We also evaluate the number of isocenters $N_{0.95}$ required to achieve the reference coverage of 95%. As shown by Table 3, the clustering method can reduce the isocenter number by 1.70 isocenters on average for the 10 patients. For two patients one more isocenter is needed, all other patient cases need less or equal. With a maximum of 50 isocenters, sphere packing fails to achieve the reference coverage in seven out of 10 cases. For the remaining three cases, the number of isocenters can be reduced by an average of 1.81. The random generation reaches 95% coverage in seven cases, but always requires more isocenters than N_{ref}, with an average of 9.38 more isocenters.

The resulting coverage of the treatment plans for two example cases is shown in Figures 4 and 5. The

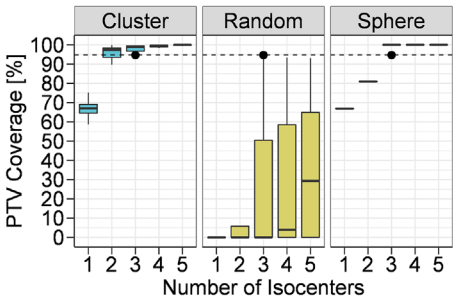

FIGURE 4 Coverage of the PTV for case 1 depending on the generation method and number of isocenters. The black point represents the results of the reference plans. PTV, planning target volume.

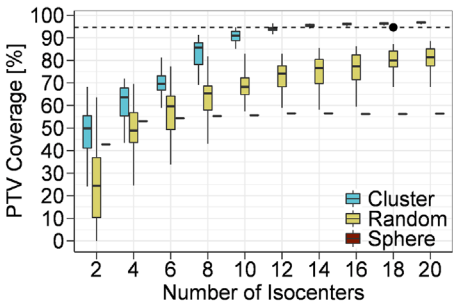

FIGURE 5 Coverage of the PTV for case 9 depending on the generation method and number of isocenters. The black point represents the results of the reference plans.

PTV coverage averaged over the 30 seeds is displayed depending on the number of generated isocenters.

Case 1 (Figure 4) represents the smallest PTV, which also has the smallest $N_{ref} = 3$. The reference isocenters result in a coverage of 0.953. For the sphere packing

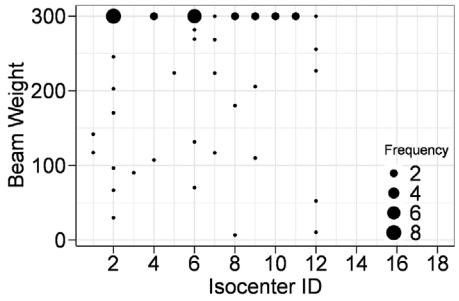

FIGURE 6 Beam weights per isocenter for case 9 with 18 isocenters generated by sphere packing. Isocenters 13–18 are not used after optimization.

TABLE 4 Index statistic if N is determined automatically.

	Clustering	Clustering + Pruning
ΔN	3.72 ± 322	− 2.46 ± 360[a]
CO	0.98 ± 002	0.97 ± 003
nCI	1.24 ± 019	1.27 ± 022
HI	2.00 ± 044	2.07 ± 046
GI	1.94 ± 021	1.93 ± 020

$\Delta N = N - N_{ref}$.
Abbreviations: CO, coverage; GI, 50% gradient index; HI, homogeneity index; nCI, new conformity index.
a*Note* that with pruning $max(\Delta N) = 0$.

algorithm a coverage of 1.00 is achieved for three or more isocenters.

Clustering achieves full coverage for four or more isocenters. With three isocenters, a coverage of 0.977 ± 0.027 is attained.

Random generation achieves 0.019 ± 0.067 (one isocenter) to 0.352 ± 0.327 (five isocenters) coverage. The standard deviation is higher than that of clustering lying between 0.067 and 0.327, compared to 0.009–0.067. Sphere packing is deterministic, therefore the standard deviation is 0.000.

Case 1 is the case with the highest deviation in conformity index for $N = N_{ref}$. The clustering results in a coverage of 1.000 and a conformity index of 2.052 compared to 0.956 coverage and a conformity index of 1.694. To compare conformity based on similar coverage, the dose limits of the shells were decreased from 7.5 and 1.6 Gy to 5.6 and 1.4 Gy, respectively. With the new shell limits, clustering results in 0.961 coverage and a 1.671 conformity index.

With $N_{ref} = 18$, case 9 (Figure 5) is the case with the most isocenters. Using those isocenters as reference leads to a coverage of 0.943 ± 0.002. Sphere packing reaches a plateau in coverage, where increasing the number of isocenters has no effect on the coverage. For eight isocenters or more, coverage is between 0.55 and 0.56. For $N = N_{ref} = 18$, sphere packing results in an average coverage of 0.554. Figure 6 shows the distribution of beam weights per isocenter for a plan with 18 isocenters generated by sphere packing. The 12 isocenters with active beams activate an average of 4.4 beams. Only one active beam is associated with each of two isocenters, and two isocenters each belong to more than 10 beams. Six of the 18 generated isocenters are not used, while clustering and random generation use an average of 17 and 15 isocenters, respectively. When using random isocenter generation or the clustering method, the achieved coverage increases with the number of generated isocenters as seen in all 10 cases. Clustering achieves a coverage above 0.95 for 13 or more isocenters.

Random generation achieves 0.134 ± 0.111 (one isocenter) to 0.805 ± 0.062 (20 isocenters) coverage. The standard deviation of the coverage is considerably higher than that of clustering, ranging from 0.062 to 0.173, compared to 0.003–0.139.

Figure 7 shows dose–volume histograms for the PTV and the cochlea for example configurations. Figure 8 shows the corresponding isodose plot with the reference and clustered isocenters for case 9.

3.2 | Determination of *N*

Table 4 gives an overview over the index statistics averaged over all 10 cases, if the number of isocenters is chosen automatically with the clustering method.

Without further pruning, the method overestimates N in eight cases with an average overestimation of 3.72 isocenters. With the additional isocenter pruning, 2.46 isocenters less than N_{ref} are used on average. The resulting coverage is only reduced by one percentage point from 98 to 97% compared to without pruning. For all 10 patients, a coverage above 95% is achieved. Conformity and homogeneity improved compared to the values achieved with $N = N_{ref}$ with clustering (see Table 2). With $N_{ref} = 18$, case 9 is the most complex. Also for pruning, this case is the one with the highest number of determined isocenters. However, with $N_c = 10$, the number of required isocenters for that case is almost halved compared to N_{ref}.

3.3 | Runtime

The computation time is mainly influenced by the time to solve the optimization problem and the beam generation as shown in Figure 9. Since the clustering method requires a preplanning step to determine the weighted beam set required for clustering, the average runtime of 43 s is 2.5 times that of sphere packing and random generation with 17 s. Runtimes for isocenter generation and optimization increase slightly with increasing N. Isocenter generation with the clustering method (0.12–0.22 s) and sphere packing (0.12–0.21s) need similar times, random selection is faster by factor 200 (0.001–0.002 s).

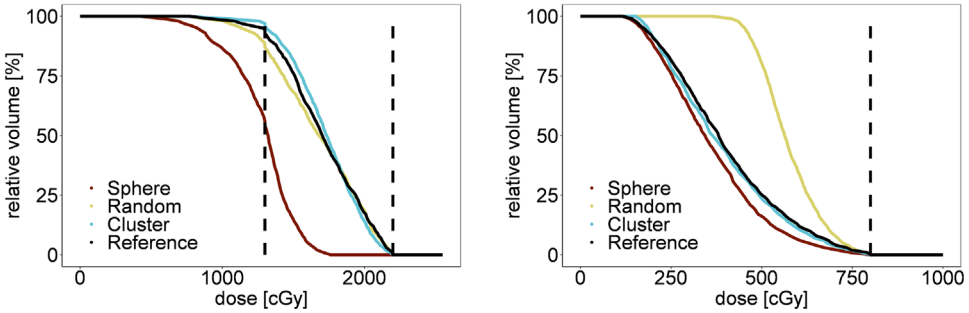

(a) PTV case 9 (b) Cochlea case 9

FIGURE 7 DVH plots of the PTV and the cochlea for case 9. The dotted lines mark the described dose, maximum PTV, and maximum cochlea dose. PTV, planning target volume.

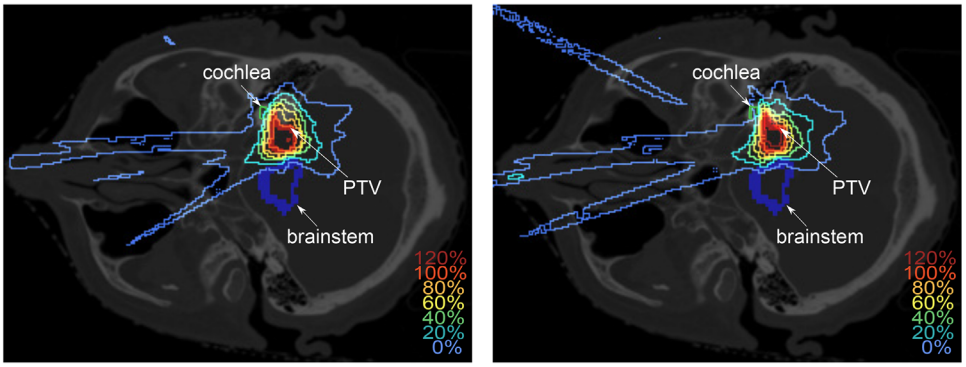

(a) Cluster (b) Reference

FIGURE 8 Isodose distribution for case 9. 100% ≙ 13 Gy.

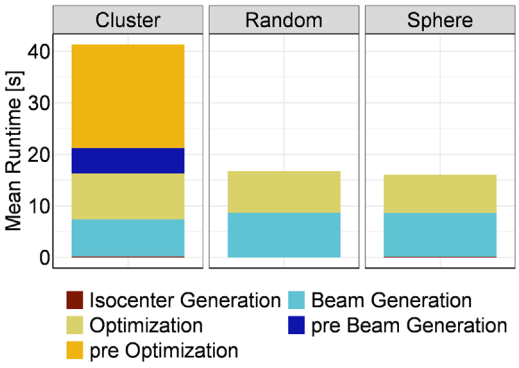

FIGURE 9 Average runtimes.

The additional pruning step adds additional 28 ± 9 s on average, which leads to a total average runtime of 75 ± 25 s.

4 | DISCUSSION

Considering Figures 3–5, we have shown that the clustering method results in greater or equal coverage compared to sphere packing and random selection methods. The random generation method is able to produce viable plans as it improves treatment plan quality with increasing N. However, to achieve clinically acceptable results, the number of isocenters needs to be increased by an average of 8.47 compared to N_{ref}, resulting in undesirable long treatment times due to repositioning. The random generation method also has a high standard deviation of up to 33% in the resulting coverage on per patient basis, illustrating a large range of possible plan qualities. A major drawback of the method is that it does not take into account the location of the isocenters relative to each other.

For the three smallest PTV sizes considered, the sphere packing approach and the clustering method can both produce clinically acceptable planning results for $N = N_{ref}$ and perform considerably better than randomly assigned isocenters. In the remaining cases, sphere packing reaches a plateau where increasing the allowed number of isocenters has no effect on coverage. There is a limit to the number of spheres packed and thus generated isocenters, given by the number at which all voxels of the target are covered. Furthermore, because of the restricting shells and OARs, some generated spheres cannot be used as needed during treatment plan optimization, resulting in a limited PTV coverage. For $N = N_{ref}$, coverage of the clustering method averages 97% with a small standard

deviation of 3 pp. Therefore, it improves coverage by 15 pp compared to sphere packing, 30 pp compared to random selection and 2 pp compared to the expert selected isocenters. The average conformity index is higher than that of the reference plans. This is primarily due to the structure of the optimization problem, where the primary goal is to maximize PTV coverage. However, the average conformity index of 1.24 remains in the range between 1 and 2, which is desired in order to comply with treatment plan requirements.[26] Note that dose constraints are tuned for the reference plans to reach 95% coverage in this study. If the constraints would be adapted for the clustering method to reach 95% coverage, improvements in the conformity index can be expected as we demonstrated for one example case.

The clustering approach's automatic determination of the number of isocenters depends on the randomly selected beam set. Nevertheless, the resulting coverage has only a low standard deviation. However, in eight out of 10 cases, N is higher than N_{ref}. Therefore, an additional pruning step was introduced, which reduces N without having a major impact on the planning results. On average, the clustering with pruning uses 2.46 fewer isocenters than N_{ref}.

Since it requires several optimization steps, the clustering method takes more than twice as long as the other two presented methods to generate a treatment plan. With the additional pruning step to automatically determine the required isocenters, the algorithm takes an average of 75 s. However, this needs to be related to the process of manual isocenter placement, which currently produces clinically preferable plans.[16] It also requires several optimization steps as centers are moved, added, or deleted iteratively until a satisfactory treatment plan is found. Especially for more complex cases, this can take an hour or longer. Therefore, the runtime of the presented clustering method has the potential to greatly reduce planning time.

We use linear programming to optimize the inverse planning problem. In principle, our approach could also be realized with different inverse optimization strategies including constrained quadratic optimization.

Previously, sphere packing has been proposed with various algorithms for Gamma-Knife radiosurgery, which are either based on quadratic programming[27] or geometrically based heuristics.[2,11,12,28–30] A nongreedy approach might lead to better results than the implemented one. However, unlike the Gamma-Knife system, which delivers beams from multiple locations at once, we showed that isocenters of the ZAP-X system are only targeted from a few distinct nodes. Furthermore, unlike the Gamma Knife, beam-on times of those beams differ. The fewer beams that intersect at a isocenter and the greater the variation in beam weighting, the less the intersecting shape resembles a sphere. As a result, a sphere packing approach as previously proposed[17] is not as well-suited to the ZAP-X, and established sphere packing methods are not expected to produce comparable good results as with the Gamma Knife. Furthermore, the methods are all limited to place the isocenter within the target volume. In contrast, in cases with irregular target geometry, it might be advantageous to place isocenters outside of the actual target. Another issue with sphere packing isocenter selection methods is that they do not consider OAR proximity when placing spheres. Both issues are not present with the proposed clustering method, making it better suited for complex cases.

5 | CONCLUSION

We presented an automatic approach for optimization of isocenter positions in gyroscopic radiation therapy.

Based on coverage, our automatic isocenter selection algorithm outperformed the other automatic approaches and an expert human planner, with satisfactory conformity and homogeneity. For highly irregular targets, many isocenters may be needed to achieve reasonable coverage, dose conformity, and homogeneity. Manual placement can be very difficult and time-consuming for a novice planner, especially for irregular target shapes that are difficult to visualize in 3D. Our approach improves plan quality while also reducing the effort required by the human planner.

ACKNOWLEDGMENTS

This work was partially funded by Deutsche Forschungsgemeinschaft (grants SCHL 1844/3-2 and SCHL 1844/6-1).

Open access funding enabled and organized by Projekt DEAL.

CONFLICT OF INTEREST STATEMENT

The authors declare no conflicts of interest.

REFERENCES

1. Wolf A, Kondziolka D. Brain metastases: radiosurgery. In: Schiff D, van den Bent MJ, eds. *Handbook of Clinical Neurology : Metastatic Disease of the Nervous System*. Elsevier; 2018;149:129-135.
2. Ghobadi K, Ghaffari HR, Aleman DM, Jaffray DA, Ruschin M. Automated treatment planning for a dedicated multi-source intracranial radiosurgery treatment unit using projected gradient and grassfire algorithms. *Med Phys*. 2012;39:3134-3141.
3. Weidlich GA, Schneider MB, Simcic V, Oostman Z, Adler JR. Self-Shielding for the ZAP-X®: revised characterization and evaluation. *Cureus*. 2021;13:e13660.
4. Kilby W, Dooley JR, Kuduvalli G, Sayeh S, Maurer CR. The CyberKnife robotic radiosurgery system in 2010. *Technol Cancer Res Treat*. 2010;9:433-452.
5. Kilby W, Naylor M, Dooley JR, Maurer CR, Sayeh S. A Technical overview of the CyberKnife system. In: Abedin-Nasab MH, ed. *Handbook of Robotic and Image-guided Surgery*. Elsevier; 2020:15-38.

6. Gayen S, Kombathula SH, Manna S, Varshney S, Pareek P. Dosimetric comparison of coplanar and non-coplanar volumetric-modulated arc therapy in head and neck cancer treated with radiotherapy. *Radiat Oncol J*. 2020;38:138-147.
7. Smyth G, Evans PM, Bamber JC, Bedford JL. Recent developments in non-coplanar radiotherapy. *Brit J Radiol*. 2019;92:20180908.
8. Schlaefer A, Schweikard A. Stepwise multi-criteria optimization for robotic radiosurgery. *Med Phys*. 2008;35:2094-2103.
9. Zeverino M, Marguet M, Zulliger C, et al. Novel inverse planning optimization algorithm for robotic radiosurgery: first clinical implementation and dosimetric evaluation. *Phys Med*. 2019;64:230-237.
10. Bhatnagar JP, Novotny J, Niranjan A, et al. First year experience with newly developed Leksell Gamma Knife Perfexion. *J Med Phys*. 2009;34:141-148.
11. Wu QJ, Bourland JD. Morphology-guided radiosurgery treatment planning and optimization for multiple isocenters. *Med Phys*. 1999;26:2151-2160.
12. Wagner TH, Yi T, Meeks SL. A geometrically based method for automated radiosurgery planning. *Int J Radiat Oncol Biol Phys*. 2000;48:1599-1611.
13. St John TJ, Wagner TH, Bova FJ, Friedman WA, Meeks SL. A geometrically based method of step and shoot stereotactic radiosurgery with a miniature multileaf collimator. *Phys Med Biol*. 2005;50:3263-3276.
14. Sjölund J, Riad S, Hennix M, Nordström H. A linear programming approach to inverse planning in Gamma Knife radiosurgery. *Med Phys*. 2019;46:1533-1544.
15. Wieczorek DJ, Kotecha R, Hall MD, et al. Systematic evaluation and plan quality assessment of the Leksell® gamma knife® lightning dose optimizer. *Medical Dosim: Off J Am Assoc Med Dosim*. 2022;47:70-78.
16. Muacevic A, Eder MM, Hofmann T, Fürweger C, Ehret F. Self-shielding gyroscopic radiosurgery—a first clinical experience, case series, and dosimetric comparison. *World Neurosurg*. 2022;164:e420-e426.
17. Adler JR, Schweikard A, Achkire Y, et al. Treatment planning for self-shielded radiosurgery. *Cureus*. 2017;9:e1663.
18. Ahnesjö A, Aspradakis MM. Dose calculations for external photon beams in radiotherapy. *Phys Med Biol*. 1999;44:R99-R155.
19. Macqueen J. Some methods for classification and analysis of multivariate observations. In: Proceedings of the 5th Berkeley Symposium on Mathematical Statistics and Probability. University of California Press; 1967:281-297.
20. Bradley PS, Fayyad Usama M. Refining initial points for K-means clustering. In: Proceedings of the Fifteenth International Conference on Machine Learning. 1998.
21. Blum H. A transformation for extracting new descriptors of shape. In: Models for the Perception of Speech and Visual Form. 1967:362-380.
22. Calinski T, Harabasz J. A dendrite method for cluster analysis. *Commun Stat Theory Methods*. 1974;3:1-27.
23. Nakamura JL, Verhey LJ, Smith V. Dose conformity of gamma knife radiosurgery and risk factors for complications. *Int J Radiat Oncol Biol Phys*. 2001;51:1313-1319.
24. Knöös T, Kristensen I, Nilsson P. Volumetric and dosimetric evaluation of radiation treatment plans: radiation conformity index. *Int J Radiat Oncol Biol Phys*. 1998;42:1169-1176.
25. Paddick I, Lippitz B. A simple dose gradient measurement tool to complement the conformity index. *J Neurosurg*. 2006;105:194-201.
26. Feuvret L, Noël G, Mazeron JJ, Bey P. Conformity index: a review. *Int J Radiat Oncol Biol Phys*. 2006;64:333-342.
27. Sutou A, Dai Y. Global optimization approach to unequal global optimization approach to unequal sphere packing problems in 3D. *J Optim Theory Appl*. 2002;114:671-694.
28. Ferris MC, Lim J, Shepard DM. An optimization approach for radiosurgery treatment planning. *SIAM J Optim*. 2002;13:921-937.
29. Wu QJ, Chankong V, Jitprapaikulsarn S, Wessels BW, Einstein DB, Mathayomchan B, Kinsella TJ. Real-time inverse planning for Gamma Knife radiosurgery. *Med Phys*. 2003;30:2988-2995.
30. Li S, Ng KL. Monte Carlo study of the sphere packing problem. *Phys A: Stat Mech Appl*. 2003;321:359-363.

How to cite this article: Stapper C, Gerlach S, Hofmann T, Fürweger C, Schlaefer A. Automated isocenter optimization approach for treatment planning for gyroscopic radiosurgery. *Med Phys*. 2023;50:5212–5221.
https://doi.org/10.1002/mp.16436